Molecular fingerprints and health risks of home-use incense burning smoke

Kai Song[1,2,#], Rongzhi Tang[3,4,#,*], Jingshun Zhang[5], Zichao Wan[1], Yuan Zhang[6], Kun Hu[1], Yuanzheng Gong[1], Daqi Lv[1], Sihua Lu[1], Yu Tan[7], Ruifeng Zhang[3,4], Ang Li[8], Shuyuan Yan[8], Shichao Yan[8], Baoming Fan[9], Wenfei Zhu[10], Chak K. Chan[3,4], Song Guo[1,2,*]

[1] State Key Joint Laboratory of Environmental Simulation and Pollution Control, International Joint Laboratory for Regional Pollution Control, Ministry of Education (IJRC), College of Environmental Sciences and Engineering, Peking University, *Beijing* 100871, China

[2] Collaborative Innovation Center of Atmospheric Environment and Equipment Technology, Nanjing University of Information Science & Technology, *Nanjing* 210044, China

[3] School of Energy and Environment, City University of Hong Kong, *Kowloon* 999077, Hong Kong, China

[4] Shenzhen Research Institute, City University of Hong Kong, *Shenzhen* 518057, China

[5] Shanghai Police College, *Shanghai* 200137, China

[6] School of Earth Science and Engineering, Hebei University of Engineering, *Handan* 056038, China

[7] School of Chemical Engineering and Technology, Sun-Yat-Sen University, *Zhuhai* 519000, China

[8] China Automotive Technology and Research Center (CATARC), *Beijing* 100176, China

[9] TECHSHIP (Beijing) Technology Co., LTD, *Beijing* 100039, China

[10] School of Energy and Power Engineering, University of Shanghai for Science and Technology, *Shanghai* 200093, China

[#] These authors contributed equally to this work.

* **Correspondence:** Rongzhi Tang: rongtang@cityu.edu.hk and Song Guo: songguo@pku.edu.cn

Abstract: The burning of incense for home use is a widespread practice that has been shown to have significant negative impacts on human health and air quality. However, there is a lack of understanding regarding its emission profiles and associated health risks. To address this knowledge gap, we utilized a state-of-the-art thermal desorption comprehensive two-dimensional gas chromatography-mass spectrometer (TD-GC×GC-MS) to (semi-)quantify the emission factors (EFs) of 317 volatile compounds and thoroughly investigate the organic profiles of incense burning smoke across a full-volatility range. Results showed that toluene (70.8 ± 35.7 μg g^{-1}) is the most abundant compound in incensing-burning smoke, followed by benzene, furfural, and phenol. Phenol, toluene, furfural, 2-furanmethanol, benzene, and benzyl alcohol are the main contributors to ozone and secondary organic aerosol (SOA) estimation. Intermediate volatility organic compounds (IVOCs) accounted for 19.2% of the total EFs, but 40.0% of the estimated SOA. Additionally, a novel pixel-based method, combined with aroma analysis, revealed that furfural can act as a key tracer of incense burning, and is responsible for the distinctive flavor of incense smoke. High bioaccumulation potential (BAP) assessment using pixel-based partition coefficient estimation revealed that acenaphthylene, dibenzofuran, and phthalate esters (PAEs) are chemicals of high-risk concern and warrant further control. Our results highlight the critical importance of investigating home-use incense burning and provide new insights into the health impacts of incense burning smoke by novel approaches.

1 Introduction

Incense burning is a prevalent custom in many cultures, especially in East and Southeast Asia (Chen et al., 2021). In modern times, incense burning for fragrance has become a frequent practice in households (Manoukian et al., 2013), while functional incense burning, such as mosquito coils, is used for specific purposes. Exposure to incense smoke is linked to adverse health effects like eye irritation, carcinogenicity, genotoxicity, and respiratory system damage (Wong et al., 2020; Yang et al., 2007, 2017). Incense is composed of fragrant materials, aromatic woods, herbs, and adhesive powders, usually available in the form of sticks and coils (Wong et al., 2020; Yadav et al., 2022). Incense burning releases multiple pollutants into the air, including particulate matter (PM), carbon monoxide (CO), volatile organic compounds (VOCs), and intermediate volatility/semi-volatile organic compounds (I/SVOCs) (Wong et al., 2020; Yang et al., 2007; Jetter et al., 2002).

Current studies mainly focus on the hazardous VOC and SVOC homologs released from incense-burning smoke. For instance, Lee et al. investigated 8 carbonyls and 11 VOCs emitted from incense burning and found that the emission factors (EFs) of traditional incense burning were higher than aromatic incense (Lee and Wang, 2004). Lu et al. detected 230 kinds of VOCs from mosquito-repellent incense burning, elucidating that alkanes, esters, aldehydes, ketones, and aromatics are predominant (Lu et al., 2020). Staub et al. measured 6 methoxy phenolics, 10 monoterpenoids, and other 21 kinds of SVOCs in the burning smoke of incense sticks, and identified cedrol as an important odor source (Staub et al., 2011). However, most of the studies have focused on VOC compounds, with less attention given to gaseous organics in the full volatility range (VOC-IVOC-SVOCs). A full-volatility organic characterization may better evaluate the ozone formation potential (OFP) and secondary organic aerosol (SOA) formation, as I/SVOCs are potentially important precursors of ozone and SOA formation (Zhao et al., 2007; Tang et al., 2021; Guo et al., 2014, 2020). Meanwhile, mapping organics from incense smoke helps to evaluate the potential health risks of toxic compounds.

Comprehensive two-dimensional gas chromatography (GC×GC) is a powerful technique dealing with the coelution problem in conventional one-dimensional gas chromatography (1D GC). Pollutants from gasoline exhaust, diesel exhaust, and cooking emissions are well separated and

identified (Drozd et al., 2019; Alam et al., 2018; Song et al., 2022a). As much as 50 ~ 98% of the total response in GC×GC chromatograms could be explained (Huo et al., 2021; Song et al., 2022b). Previous work identified 324 compounds from incense smoke by coupling solid-phase microextraction (SPME) with GC×GC, yet chemicals are not quantified (Tran and Marriott, 2007). Thus, a non-targeted and quantitative assessment of incense burning emissions is currently lacking.

In this work, two types of incense sticks and three kinds of incense coils were burned in a steel chamber. Gaseous pollutants were trapped by Tenax TA desorption tubes and then analyzed by a thermal desorption comprehensive two-dimensional gas chromatography-mass spectrometer (TD-GC×GC-MS). Pixel-based multiway principal component analysis (MPCA) was utilized to identify markers of incense burning. Risk assessment of pollutants from incense burning emissions was then evaluated by pixel-based approaches and high-risk compounds related to incense burning were assessed.

2 Methodology

2.1 Sampling and instrumentation

Incenses were purchased from the market, including 4 common incense sticks, 2 Thailand incense sticks, 1 mosquito coil, and 2 incense coils (Figure S1). Incenses could also be classified by their material, containing 2 aromatic coils, 4 aromatic sticks, 1 mosquito coil, 1 sandalwood stick, and 1 smokeless sandalwood stick (Figure S1). Incenses were burned in a stainless combustion chamber (1 m^3). After ignition, the burning incense changed from flaming to smoldering. Each kind of incense was burned at least twice. Incenses were weighed before and after combustion. Preconditioned Tenax TA desorption tubes (Gerstel 6 mm 97 OD, 4.5 mm ID glass tube) were utilized to trap organics with a sampling flow of 0.2 L min^{-1}.

A comprehensive two-dimensional gas chromatography-quadrupole mass spectrometer (GC×GC-qMS, GC-MS TQ8050, Shimadzu, Japan) coupled with a thermal desorption system (TDS 3 C506, Gerstel, Germany) was used for sample analysis. The desorption temperature was 280 ℃. The cooled injection system (CIS) with a Tenax TA liner was held at 20 ℃ and ramped to 320 ℃ once injecting the gaseous sample into GC columns. The column combination was SH-Rxi-1ms (1^{st}, 30 m × 0.25 mm × 0.25 μm) and BPX50 (2^{nd}, 2.5 m × 0.1 mm × 0.1 μm). The modulation period was

6s. See Table S1 and elsewhere (Song et al., 2022a) for more information.

2.2 Chemical identification, quantification, and 2D binning

A series of standard mixtures (2 μg mL^{-1}, 5 μg mL^{-1}, 10 μg mL^{-1}, 20 μg mL^{-1}, 40 μg mL^{-1} in CH_2Cl_2) was injected into Tenax TA tubes (2 μL). After purging the solvent with nitrogen gas, the standards were thermally desorbed. The standard mixture contains 26 *n*-alkanes (C7 - C32, CNW Technologies, ANPEL Laboratory Technologies (Shanghai) Inc., China), 16 PAHs, 11 phenolic compounds, 9 alcohols, 4 aldehydes, 8 aromatics, 24 esters, 7 ketones, 5 siloxanes, and 39 other compounds. Gaseous organics are quantified by external calibration curves with most of the R^2 between 0.95 and 0.999 (Table S2). Chemicals with the same retention times and mass spectrums were directly qualified and quantified. The unidentified chemicals were qualified by matching their mass spectrum with library spectrums in the National Institute of Standard Technology library (NIST 17). Reverse factors of more than 700 were acceptable in this work. As homologs on the two-dimensional chromatogram (contour plot) were eluted with near-equal one-dimensional intervals, chemicals were then qualified by combing the location of the contour plot and the mass spectrums (Song et al., 2023). Compounds without standards were semi-quantified by *n*-alkanes from the same volatility bin (uncertainty 69%) and surrogates from the same chemical class (uncertainty 27%). Instrument detection limits (IDLs) for organics semi-quantified were unknown, as a result, chemicals with negative values calculated by calibration curves were quantified by the volume-to-mass (ng) ratio of the lowest quantification point of standards (Table S2). A total of 317 chemicals were (semi)-quantified, including 10 acids, 34 alcohols, 19 aldehydes, 25 aromatics, 38 esters, 49 ketones, 18 *n*-alkanes, 26 nitrogen-containing compounds, and 10 phenols (Table S3).

The compounds identified were sliced into two-dimensional bins (2D bins) (Song et al., 2022a). 1^{st} retention times are linked to the volatility of species (B8 to B31 with decreasing volatility) while 2^{nd} retention times are associated with polarity (P1 to P8 with increasing polarity). Emission factors of compounds in the same 2D bin were aggregated (Table S3).

2.3 Emission factor (EF), ozone formation potential (OFP), and secondary organic aerosol (SOA) estimation

The emission factor (EF, μg g^{-1}) was calculated by the following equation:

$$EF = \frac{m\,V}{ftM} \quad (1)$$

m is the absolute mass of pollutants (μg) captured by Tenax TA tubes. V is the volume of the steel chamber (1 m^3). The sampling flow and duration of the Tenax TA tube are f (0.0002 m^3 min^{-1}) and t (min), respectively. M is the combustion mass (g) of the incense. The sampling volume of Tenax TA tubes (0.003 ~ 0.01 m^3) was significantly smaller than the total volume of the steel chamber (1 m^3) and the volume change of the chamber could be neglected.

The ozone formation potential (OFP, μg g^{-1}) was calculated using equation (2). EF_i is the emission factor of precursor i (μg g^{-1}) with maximum incremental reactivity (MIR) of MIR_i. The OFP was calculated inside the FOQAT packages developed by Tianshu Chen (https://github.com/tianshu129/foqat). The MIR used in this work can be found in Table S3.

$$OFP = \sum[EF_i] \times MIR_i \quad (2)$$

Secondary organic aerosol (SOA) was estimated by equation (3).

$$SOA = \sum[EF_i] \times (1 - e^{-k_{OH,i} \times [OH] \times \Delta t}) \times Y_i \quad (3)$$

Where $k_{OH,i}$ and $Y_i$represent the OH reaction rate and SOA yield of precursor i, respectively (Table S3). The SOA yields of precursors were from literature (Loza et al., 2014; Harvey and Petrucci, 2015; Tkacik et al., 2012; Shah et al., 2020; McDonald et al., 2018; Chan et al., 2010, 2009; Wu et al., 2017; Li et al., 2016; Matsunaga et al., 2009; Algrim and Ziemann, 2019, 2016; Liu et al., 2018; Charan et al., 2020) or surrogates from *n*-alkanes in the same volatility bins (Zhao et al., 2017). k_{OH} and Y could be found in Table S3. $[OH] \times \Delta t$ is the OH exposure and was set to be 13 $\times 10^{10}$ molecules cm^{-3}s (24 hours in OH concentration of 1.5 $\times 10^6$ molecules cm^{-3}).

2.4 Pixel-based risk assessments of incense-burning pollutants

Octanol-air partition coefficient (K_{o-a}), air-water partition coefficient (K_{a-w}), and octanol-water partition coefficient (K_{o-w}) were estimated by a linear free-energy relationship (LFER) model (Nabi et al., 2014; Zushi et al., 2019). Partition coefficients of chemicals are associated with their two-dimensional retention times (Song et al., 2022b). Chemicals with high bioaccumulation potential (BAP) are defined as contaminants with partition coefficients of ($2 < \log K_{o\text{-}w} < 11$) and ($6 < \log K_{o\text{-}a} < 12$). See Zushi et al. (Zushi et al., 2019) for more information. The R source code was obtained from GitHub (https://github.com/Yasuyuki-Zushi).

3 Results and discussions

3.1 Emission profiles of different incense-burning organics

Figure S2 is a typical chromatogram of incense burning emissions, which is also set as the reference chromatogram during the pixel-based analysis. As much as 90.2% of the total percent response could be explained. The ratio is similar to a recent study resolving biomass burning emissions (98%) (Huo et al., 2021). The emission factor (EF) of total organics is 791.8 ± 300.6 μg g^{-1}, consistent with previous work (100 ~ 19100 μg g^{-1}) (Lee and Wang, 2004), and comparable to rice (475.9 ± 61.2 μg g^{-1}), pine (558.6 ± 103.6 μg g^{-1}) and poplar (564.6 ± 124.1 μg g^{-1}) combustions (Zhu et al., 2022), but much lower than coal combustion (6.3 mg g^{-1}) (Huo et al., 2021). The contributions of different chemical categories are displayed in Figure S3. Oxygenated compounds dominate the total EFs, accounting for 48.4%, followed by aromatics (29.8%), *b*-alkanes (5.3%), nitrogen-containing compounds (4.0%), alkenes (4.0%), and *n*-alkanes (2.3%). Unresolved complex mixtures (UCMs) are further separated into aliphatic, cyclic, and oxygenated UCM due to retention times and mass spectrums. The UCM ratio in this work (2.3% in EFs) is comparable to biomass burning (Huo et al., 2021) and diesel exhaust (He et al., 2022) analyzed by GC×GC-MS, and is much smaller than the UCM ratio (>50%) in biomass burning smoke analyzed by 1D GC-MS (Zhu et al., 2022). Ketones are the most abundant oxygenated compounds, accounting for 13.6% of the total EFs, followed by aldehydes (9.7%), esters (8.1%), alcohols (6.9%), phenols (3.6%), and acids (3.1%). The emission profiles are comparable to corncob and wood combustion, which are also dominated by ketones and esters (Huo et al., 2021). However, the abundance of phenol is much lower than in biomass-burning smoke (>15%) (Zhu et al., 2022; Huo et al., 2021), while comparable to coal combustion (5.4%) (Huo et al., 2021).

EFs of selected compounds are listed in Table S4, which were comparable with other incense burning studies (Lee and Wang, 2004; Yang et al., 2007; Manoukian et al., 2016), while the EF of benzene (59.6 ± 43.1 μg g^{-1}) is slightly lower than other studies (188 ~ 1826 μg g^{-1}) (Lee and Wang, 2004; Yang et al., 2007; Manoukian et al., 2016). The Tenax TA liner in the CIS system does not capture benzene at an initial temperature of 20 ℃, while it is efficient for the trapping of most I/SVOC compounds. Lower CIS temperature may trap benzene while causing water condensation.

As a result, the tailing of benzene on the second column (Figure S2) causes an underestimation of blob integration and results in an underestimation of EF.

The top 10 compounds are all VOC compounds (Figure S4), accounting for 35.3% of the total EFs. Toluene (70.8 ± 35.7 μg g^{-1}) is the most abundant compound in incensing-burning smoke, followed by benzene, furfural, phenol, styrene, 2-oxo-propanoic acid methyl ester, 3-methyl-2-butanone, ethylbenzene, 1-hydroxy-2-propanone, and benzyl alcohol. Note that VOC compounds discussed here are part of volatile organics captured by Tenax-TA, not the common VOCs detected by SUMMA-GC-MS. The top 5 IVOCs are B17 *b*-alkanes, B16 *b*-alkanes, B18 *b*-alkanes, diethyl phthalate, and 1,6-dioxacyclododecane-7,12-dione. The naphthalene (a typical PAH, 2 rings) EF is 3.0 ± 1.5 μg g^{-1}, comparable to rice straw combustion (Zhu et al., 2022). SVOCs are all *n*-alkane species and only account for less than 1% of the total EFs.

The average VBS distribution of incense burning is displayed in Figure 1, and the volatility-polarity distribution is exhibited in Figure S5. In general, the EF decreases as the volatility decreases, following the trend of VOC-EF (80.8%) > IVOC-EF(19.2%) >> SVOC-EF (<0.1%). The chemical compositions in the VOC-IVOC range are shown in Figure S6. Oxygenated compounds (53.5% of the total VOC EFs) and aromatics (37.6%) are largely detected in the VOC range, while *b*-alkanes, *n*-alkanes, and oxygenated compounds are the main components of IVOC compounds. The average VBS distribution is similar to cooking emissions (Song et al., 2022a) and wood combustion (Stewart et al., 2021), but less volatile than gasoline exhausts (Lu et al., 2018) and more volatile than diesel emissions (Lu et al., 2018). For example, the proportion of chemicals with saturated vapor concentration (C*) more than 10^6 μg m^{-3} (Figure 1 a) is 80.8% (incense burning), 80.7% (cooking emissions) (Song et al., 2022a), 77.6% (wood combustion) (Stewart et al., 2021), 94.2% (gasoline exhaust) (Lu et al., 2018), and 41.0% (diesel exhaust) (Lu et al., 2018). The polarity of incense burning is dominated by non-polar and intermediate-polarity organics (P1 ~ P5, Figure S5). The volatility-polarity distribution of incense burning is quite similar to cooking emissions (Song et al., 2022a), dominant by VOCs in the volatility range of before B13 and the polarity range of P1 ~ P5.

A similar emission pattern but different EFs of different incense-burning emissions are observed.

Similarities among incense burning are more dominant than diversities. First, pixel-based partial least squares-discriminant analysis (PLS-DA) elucidates that there is no systemic difference between different chromatograms of incense burning emission, no matter different incense shapes (Figure S7) or materials (Figure S8). Second, the compositions of different types of incense emissions are indeed quite similar (Figure S9 and Figure S10). Third, the multiway principal component analysis (MPCA) positive loadings are much larger than negative loadings, indicating that the similarities between samples are much more important than the differences (Figure 2).

However, the absolute EFs significantly diverge according to different incense forms (p = 0.03, Figure S11) and different materials (p < 0.01, Figure S12). Incense made in stick form (incense stick: 893.2 ± 335.6 μg g^{-1}, Thailand incense stick: 877.5 ± 123.8 μg g^{-1}) emits more organics than made in coil form (incense coil: 835.5 ± 306.0 μg g^{-1}). The EF of mosquito coil is the smallest (382.5 ± 175.0 μg g^{-1}). A similar pattern was observed in previous work (Jetter et al., 2002). Concerning the incense materials, we spot that the so-called smokeless sandalwood stick emits more abundant organics (1195.8 ± 83.3 μg g^{-1}) than common sandalwood sticks (633.7 ± 6.6 μg g^{-1}). The emission of smokeless sandalwood sticks is even greater than aromatic sticks (893.2 ± 335.6 μg g^{-1}) and coils (824.8 ± 228.5 μg g^{-1}). Our results demonstrate that although smokeless sandalwood stick is preferred as fewer particulates are generated during the combustion process, the gaseous emissions are enhanced compared to other incenses.

3.2 Contributions of home-use incense burning to ozone and secondary organic aerosols (SOA)

The total OFP is 1513.4 ± 551.0 μg g^{-1} which is 1.91 g O_3/g VOC-IVOCs. The OFP enhancement ratio (OFP per mass of precursor) is much smaller than gasoline exhaust (3.53 g O_3/g VOCs) (Wang et al., 2013) and evaporation (2.3 ~ 4.9 g O_3/g VOC) (Yue et al., 2017), showing that incense burning is less efficient on ozone formation than gasoline-related sources. The lack of IVOC measurements in previous work could also cause an overestimation of the OFP enhancement ratio as IVOCs are less efficient in ozone formation. Toluene, furfural, *p*-xylene, benzyl alcohol, phenol, 2-furanmethanol, *o*-xylene, ethylbenzene, 1-hydroxy-2-propanone, and benzene are top 10 species that contribute most to OFP (Figure S4). Oxygenated compounds take up 48.2% of the total OFP,

followed by aromatics (41.0%), and alkenes (6.7%) (Figure S3). VOCs dominate the total OFP, accounting for 92.4% while IVOCs take up 7.6% (Figure 1). Aromandendrene, naphthalene, and α-cedrene are the top 3 IVOC-OFP contributors. The volatility distribution of OFP contribution is comparable to cooking emissions, as VOCs account for 88.8 ~ 99.9% of the total cooking OFP estimation (Song et al., 2022a). Toluene contributes the most OFP in both cooking emissions and incense burning. Short-chain linear aldehydes (pentanal, hexanal, nonanal) originating from the degradation of oils play a more important role in OFP contribution in cooking emissions (Song et al., 2022a), while benzenes, furfural, alcohols, and phenols are non-negligible OFP contributors in incense burning.

Figure 1 shows the volatility distribution of estimated SOA estimation, with the top 10 contributors displayed in Figure S4. IVOCs contribute 19.2% of the EFs while accounting for 40.0% of the total SOA estimation, highlighting the importance of IVOCs in SOA formation. The contribution of IVOC species to SOA is higher than EFs due to the relatively higher yields and k_{OH}, which has already been reported in cooking emissions (Song et al., 2022a; Yu et al., 2022), gasoline exhaust (Zhao et al., 2014), diesel exhaust (Zhao et al., 2015), and biomass burning (Stewart et al., 2021). Oxygenated compounds account for 32.9% of the SOA estimation, followed by aromatics (23.7%), and *b*-alkanes (11.5%) (Figure S3). Phenol, benzyl alcohol, styrene, toluene, B18 cyclic UCM, aromandendrene, 2-furanmethanol, B17 *b*-alkanes, benzene, and phenyethyne are the top 10 SOA contributors. The incense-burning SOA formation profiles are distinct from cooking emissions (Song et al., 2022a) and biomass burning (Huo et al., 2021). Cooking SOA is largely derived from the oxidation of short-chain acids and aromatics (Song et al., 2022a), while phenols account for more than 65% of the SOA estimation from biomass burning (Huo et al., 2021). Phenols only account for 11.0% of SOA estimation in this work. Alcohols (7.3%) and furans (7.6%) are much more important SOA precursors in incense burning compared to biomass burning and cooking emissions. Compared with other sources, we stress the importance of incense-burning benzenes, furfural, alcohols, and phenols in OFP formation and alcohols and furans in SOA formation. The secondary formation potential of mosquito coils is the lowest, while OFP and SOA of burning smokeless sandalwood sticks are the highest. Compared to other incense, the higher aromatic contents of smokeless

sandalwood sticks burning fumes result in much more ozone and SOA formation.

3.3 Identification of molecular markers from incense burning

Pixel-based MPCA is utilized to identify tracers of incense burning emissions. In brief, MPCA decomposes a matrix *X* into a scoring matrix (*S*) and a loading matrix (*L*). Similarities and differences in chromatograms are revealed by positive and negative loadings, respectively (Figure 2) (Song et al., 2022b). The similarities of chromatograms could be explained by benzenes (toluene, *p*-xylene, *o*-xylene, and ethylbenzene), ketones (3-methyl-2-cyclopenten-1-one, 2-hydroxy-2-cyclopenten-1-one, 3-ethyl-2-pentanone), aldehydes (furfural, succindialdehyde, 2-methyl-2-butenal), 2-methyl-propanoic acid, 1-methyl-1H-pyrazole, 2(5H)-furanone, and 2-furanmethanol. The differences between samples could be largely explained by 2-methyl-2-butenal, 2(5H)-furanone, 3,4-dimethylfuran, 2,3-dihydro-1H-inden-1-one, 2-methoxy-naphthalene, and 1,2-dihydro-2,2,4-trimethyl-quinoline. The negative loadings (0.006) are significantly smaller than the positive loadings (0.07), confirming the dominance of similarities among chromatograms. The relationship between the EFs of these compounds among different incense types is displayed in Figure S13. Although the total EFs are significantly different (p = 0.03), the EFs of selected compounds (2-hydroxy-2-cyclopenten-1-one, 2-furanmethanol, 3-ethyl-2-pentanone, and furfural are significantly no different (p > 0.08). As a result, we recommend these compounds as incense-burning tracers. It is reported that furfural is formed during the thermal degradation of hemicelluloses (Uhde and Salthammer, 2007), while the oxidation of furfural under harsher conditions forms 2(5H)-furanone (Depoorter et al., 2021). The formation mechanism of furfural from xylose and D-xylopyranose is displayed in Figure S14 (Ahmad et al., 1995; Bonner and Roth1, 1959; Nimlos et al., 2006). The initiation of the degradation of five-carbon sugars is from the acyclic form of pentoses or directly via a 2,3-(α,β-)unsaturated aldehyde. The dehydrating of the intermediate compounds finally forms furfural (Figure S14). The addressed tracers, furfural, 2-furanmethanol, and 2(5H)-furanone, have already been identified in incense burning smoke in previous work (Depoorter et al., 2021; Tran and Marriott, 2007).

Furthermore, we compare the chemical profiles with an odor database (Aroma Office 2D, Gerstel). Among the top 20 chemicals contributing to EFs, furfural (bread-like, alcoholic,

incense-like), phenol (mushroom, acid, burnt plastics), 1-hydroxy-2-propanone (buttery, caramellic, fruity), benzyl alcohol (burning taste, flower, roasted), limonene (citrus-like, fruity, lemon-like), and 2-methyl-propanoic acid (apple-like, cheese-like, sweat) could be the aroma compounds. As for tracers identified above, 2-furanmethanol (burnt sugar, honey, sweet) could also be another aroma compound. Among them, furfural is widely and largely detected which could be the most important molecular marker of incense burning (Silva et al., 2021; Ho and Yu, 2002). Note that aromandendrene, a cucumber-like, woody, and floral compound, is only detected in one incense coil sample (incense coil 2, Figure S1). Aromandendrene is also detected in plants, such as in dry flowers of *Lonicera japonica* (Shang et al., 2011). The emission factor of aromandendrene is rather large (4.3 μg g^{-1}, 0.7% of the total EFs), and is a significant SOA precursor (2.3 μg g^{-1}, 3.9% of the total SOA estimation). The importance of aromandendrene on incense flavor and SOA formation could not be neglected. Aromandendrene could also be responsible for the distinct flavor of a certain incense coil. As above said, we recommend furfural be used as a molecular indicator of incense burning regardless of the incense type or additives, especially responsible for the flavor of incense burning.

3.4 Risk assessment of incense burning organics

The hazardous compounds from incense burning could cause adverse health effects on human health (Wong et al., 2020; Yang et al., 2007; Chen et al., 2021; Yang et al., 2017). To evaluate the potential risks of these compounds, we conducted a pixel-based risk assessment (bioaccumulation potential, BAP) for partition coefficient estimation. Chemicals with high BAP concerns are listed in Figure 3. 2-methoxy-naphthalene, acenaphthylene, dibenzofuran, diethyl phthalate, dibutyl phthalate, benzoic acid 2-ethylhexyl ester, C15 – C19 *n,* and *b*-alkanes are regarded as high BAP concern (Figure 3). Among them, acenaphthylene is a toxic polycyclic aromatic hydrocarbon (PAH) that is widely detected in incense smoke (Yadav et al., 2022). Dibenzofuran, an oxygenated compound with detrimental effects on human health (Suzuki et al., 2021), is also detected in the smoke of incense burning (Tran and Marriott, 2007). Diethyl phthalate and dibutyl phthalate are phthalate esters (PAEs) widely used as plasticizers which are endocrine disruptors (Wang and Qian, 2021). PAEs are abundant in incense smoke (Tran and Marriott, 2007). We propose that acenaphthylene, dibenzofuran, and PAEs could be chemicals of high-risk concern in incense smoke. We also assess the arctic

contamination potential (ACP) as shown in Text S1. Further epidemiologic studies should be carried on to demonstrate the health effect of these hazardous compounds.

4 Implication

The non-target approach of GC×GC-MS gives us a full glimpse of incense smoke, spotting a large pool of organics (317 compounds) covering the VOC-IVOC-SVOC range. We have provided a detailed description of both primary emission and secondary estimation of incense burning organics which is ready-to-use in SOA simulation models. IVOCs (130 compounds) are crucial organics accounting for 19.2% of the total EFs and 40.0% of the SOA estimation, highlighting the importance of incorporating IVOCs into SOA models. Further investigation should be carried on to elucidate emission characteristics of short-chain compounds that are lacking in our research, such as alkanes (<C7), alkenes (<C7), and aldehydes (<C5). By combining data obtained from gas-chromatography-flame ionization detector (GC-FID) and proton transfer mass spectrometer (PTR-MS), the emission pattern of incense burning could be well demonstrated. Comparisons of IVOC capture efficiency on different sampling materials should also be taken into account to obtain a reliable quantification result of IVOC species. High-time resolution measurement should also be carried on to understand the time-resolved pattern of incense burning.

We also suggest furfural as the molecular marker of incense burning as the EFs of furfural among samples are relatively stable. Pixel-based MPCA also indicates that furfural is responsible for the similarities between chromatograms. Furfural may be the key aroma compound of incense smoke. This key component identified in this work could be implemented in source apportionment. Furfural is also a key component contributing to OFP (rank 2). Phenol, toluene, 2-furanmethanol, benzene, and benzyl alcohol are the main contributors to both OFP and SOA.

Surprisingly, we find that the EF of burning smokeless sandalwood sticks is the highest, with a remarkable contribution to OFP and SOA, due to the high aromatic contents. We recommend that both gaseous and particulate organics should also be taken into consideration when burning incense. The single reduction of particles does not mean fewer emissions of gas-phase organics. A comprehensive assessment of incense-burning organics in both gas- and particle-phase should be implemented.

Combing pixel-based property estimation and blob identification, the risk assessment analysis of compounds could benefit analysts with less experience with GC×GC. The risk assessment in this work demonstrates that acenaphthylene, dibenzofuran, and PAEs are chemicals of high-risk concern and warrant further control. It was reported that more than half of Chinese residents burn incense every day at home for more than 20 years (Salvi and Apte, 2016). The toxic PAHs detected in indoor air could be 19 times higher than in outdoor air (Salvi and Apte, 2016). Exposure to these hazardous compounds could result in significant health threats. As a result, it is of vital importance to reveal and assess the epidemiological influences of incense burning in future work.

Acknowledgment

This research is supported by the National Natural Science Foundation of China (No. 22221004, 42107115, 42275104, 41977179), the Natural Science Foundation of Shandong Province, China (No. ZR2021QD111), the Hong Kong Research Grants Council (No. 11304121) and the special fund of State Key Joint Laboratory of Environment Simulation and Pollution Control (No. 22Y01SSPCP).

Reference

Ahmad, T., Kenne, L., Olsson, K., and Theander, O.: The formation of 2-furaldehyde and formic acid from pentoses in slightly acidic deuterium oxide studied by 1H NMR spectroscopy, Carbohydr Res, 276, 309–320, https://doi.org/10.1016/0008-6215(95)00176-T, 1995.

Alam, M. S., Zeraati-Rezaei, S., Liang, Z., Stark, C., Xu, H., MacKenzie, A. R., and Harrison, R. M.: Mapping and quantifying isomer sets of hydrocarbons (≥C12) in diesel exhaust, lubricating oil and diesel fuel samples using GC× GC-ToF-MS, Atmos Meas Tech, 11, 3047–3058, https://doi.org/10.5194/amt-11-3047-2018, 2018.

Algrim, L. B. and Ziemann, P. J.: Effect of the Keto Group on Yields and Composition of Organic Aerosol Formed from OH Radical-Initiated Reactions of Ketones in the Presence of NOx, Journal of Physical Chemistry A, 120, 6978–6989, https://doi.org/10.1021/acs.jpca.6b05839, 2016.

Algrim, L. B. and Ziemann, P. J.: Effect of the Hydroxyl Group on Yields and Composition of Organic Aerosol Formed from OH Radical-Initiated Reactions of Alcohols in the Presence of NOx, ACS Earth Space Chem, 3, 413–423, https://doi.org/10.1021/acsearthspacechem.9b00015, 2019.

Bonner, W. A. and Roth1, M. R.: The Conversion of d-Xylose-l-C14 into 2-Furaldehyde-α-C14, J Am Chem Soc, 81, 5454–5456, https://doi.org/10.1021/ja01529a051, 1959.

Chan, A. W. H., Kautzman, K. E., Chhabra, P. S., Surratt, J. D., Chan, M. N., Crounse, J. D., Kürten, A., Wennberg, P. O., Flagan, R. C., and Seinfeld, J. H.: Secondary organic aerosol formation from photooxidation of naphthalene and alkylnaphthalenes: Implications for oxidation of intermediate volatility organic compounds (IVOCs), Atmos Chem Phys, 9, 3049–3060, https://doi.org/10.5194/acp-9-3049-2009, 2009.

Chan, A. W. H., Chan, M. N., Surratt, J. D., Chhabra, P. S., Loza, C. L., Crounse, J. D., Yee, L. D., Flagan, R. C., Wennberg, P. O., and Seinfeld, J. H.: Role of aldehyde chemistry and NOx concentrations in secondary organic aerosol formation, Atmos Chem Phys, 10, 7169–7188, https://doi.org/10.5194/ACP-10-7169-2010, 2010.

Charan, S. M., Buenconsejo, R. S., and Seinfeld, J. H.: Secondary organic aerosol yields from the oxidation of benzyl alcohol, Atmos Chem Phys, 20, 13167–13190, https://doi.org/10.5194/acp-20-13167-2020, 2020.

Chen, K. S. F., Tsai, Y. P., Lai, C. H., Xiang, Y. K., Chuang, K. Y., and Zhu, Z. H.: Human health-risk assessment based on chronic exposure to the carbonyl compounds and metals emitted by burning incense at temples, Environmental Science and Pollution Research, 28, 40640–40652, https://doi.org/10.1007/s11356-020-10313-1, 2021.

Depoorter, A., Kalalian, C., Emmelin, C., Lorentz, C., and George, C.: Indoor heterogeneous photochemistry of furfural drives emissions of nitrous acid, Indoor Air, 31, 682–692, https://doi.org/10.1111/INA.12758, 2021.

Drozd, G. T., Zhao, Y., Saliba, G., Frodin, B., Maddox, C., Oliver Chang, M. C., Maldonado, H., Sardar, S., Weber, R. J., Robinson, A. L., Goldstein, A. H., Chang, M. C. O., Maldonado, H., Sarder, S., Weber, R. J., Robinson, A. L., Goldstein, A. H., Oliver Chang, M. C., Maldonado, H., Sardar, S., Weber, R. J., Robinson, A. L., and Goldstein, A. H.: Detailed Speciation of Intermediate Volatility and Semivolatile Organic Compound Emissions from Gasoline Vehicles: Effects of Cold-Starts and Implications for Secondary Organic Aerosol Formation, Environ Sci Technol, 53, 1706–1714, https://doi.org/10.1021/acs.est.8b05600, 2019.

Guo, S., Hu, M., Zamora, M. L., Peng, J., Shang, D., Zheng, J., Du, Z., Wu, Z., Shao, M., Zeng, L., Molina, M. J., and Zhang, R.: Elucidating severe urban haze formation in China, Proc Natl Acad Sci U S A, 111, 17373–17378, https://doi.org/10.1073/pnas.1419604111, 2014.

Guo, S., Hu, M., Peng, J., Wu, Z., Zamora, M. L., Shang, D., Du, Z., Zheng, J., Fang, X., Tang, R., Wu, Y., Zeng, L., Shuai, S., Zhang, W., Wang, Y., Ji, Y., Li, Y., Zhang, A. L., Wang, W., Zhang, F., Zhao, J., Gong, X., Wang, C., Molina, M. J., and Zhang, R.: Remarkable nucleation and growth of ultrafine particles from vehicular exhaust, Proc Natl Acad Sci U S A, 117, 3427–3432, https://doi.org/10.1073/pnas.1916366117, 2020.

Harvey, R. M. and Petrucci, G. A.: Control of ozonolysis kinetics and aerosol yield by nuances in the molecular structure of volatile organic compounds, Atmos Environ, 122, 188–195, https://doi.org/10.1016/j.atmosenv.2015.09.038, 2015.

He, X., Zheng, X., You, Y., Zhang, S., Zhao, B., Wang, X., Huang, G., Chen, T., Cao, Y., He, L., Chang, X., Wang, S., and Wu, Y.: Comprehensive chemical characterization of gaseous I/SVOC emissions from heavy-duty diesel vehicles using two-dimensional gas chromatography time-of-flight mass

425 spectrometry, Environmental Pollution, 305, 119284, https://doi.org/10.1016/j.envpol.2022.119284,
426 2022.
427 Ho, S. S. H. and Yu, J. Z.: Concentrations of formaldehyde and other carbonyls in environments
428 affected by incense burning, Journal of Environmental Monitoring, 4, 728–733,
429 https://doi.org/10.1039/b200998f, 2002.
430 Huo, Y., Guo, Z., Liu, Y., Wu, D., Ding, X., Zhao, Z., Wu, M., Wang, L., Feng, Y., Chen, Y., Wang, S.,
431 Li, Q., and Chen, J.: Addressing Unresolved Complex Mixture of I/SVOCs Emitted From Incomplete
432 Combustion of Solid Fuels by Nontarget Analysis, Journal of Geophysical Research: Atmospheres,
433 126, e2021JD035835, https://doi.org/10.1029/2021JD035835, 2021.
434 Jetter, J. J., Guo, Z., McBrian, J. A., and Flynn, M. R.: Characterization of emissions from burning
435 incense, Science of the Total Environment, 295, 51–67,
436 https://doi.org/10.1016/S0048-9697(02)00043-8, 2002.
437 Lee, S. C. and Wang, B.: Characteristics of emissions of air pollutants from burning of incense in a
438 large environmental chamber, Atmos Environ, 38, 941–951,
439 https://doi.org/10.1016/j.atmosenv.2003.11.002, 2004.
440 Li, L., Tang, P., Nakao, S., and Cocker, D. R.: Impact of molecular structure on secondary organic
441 aerosol formation from aromatic hydrocarbon photooxidation under low-NOx conditions, Atmos
442 Chem Phys, 16, 10793–10808, https://doi.org/10.5194/acp-16-10793-2016, 2016.
443 Liu, T., Wang, Z., Huang, D. D., Wang, X., and Chan, C. K.: Significant Production of Secondary
444 Organic Aerosol from Emissions of Heated Cooking Oils, Environ Sci Technol Lett, 5, 32–37,
445 https://doi.org/10.1021/acs.estlett.7b00530, 2018.
446 Loza, C. L., Craven, J. S., Yee, L. D., Coggon, M. M., Schwantes, R. H., Shiraiwa, M., Zhang, X.,
447 Schilling, K. A., Ng, N. L., Canagaratna, M. R., Ziemann, P. J., Flagan, R. C., and Seinfeld, J. H.:
448 Secondary organic aerosol yields of 12-carbon alkanes, Atmos Chem Phys, 14, 1423–1439,
449 https://doi.org/10.5194/acp-14-1423-2014, 2014.
450 Lu, F., Li, S., Shen, B., Zhang, J., Liu, L., Shen, X., and Zhao, R.: The emission characteristic of VOCs
451 and the toxicity of BTEX from different mosquito-repellent incenses, J Hazard Mater, 384, 121428,
452 https://doi.org/10.1016/j.jhazmat.2019.121428, 2020.

Lu, Q., Zhao, Y., and Robinson, A. L.: Comprehensive organic emission profiles for gasoline, diesel, and gas-turbine engines including intermediate and semi-volatile organic compound emissions, Atmos Chem Phys, 18, 17637–17654, https://doi.org/10.5194/acp-18-17637-2018, 2018.

Manoukian, A., Quivet, E., Temime-Roussel, B., Nicolas, M., Maupetit, F., and Wortham, H.: Emission characteristics of air pollutants from incense and candle burning in indoor atmospheres, Environmental Science and Pollution Research, 20, 4659–4670, https://doi.org/10.1007/s11356-012-1394-y, 2013.

Manoukian, A., Buiron, D., Temime-Roussel, B., Wortham, H., and Quivet, E.: Measurements of VOC/SVOC emission factors from burning incenses in an environmental test chamber: influence of temperature, relative humidity, and air exchange rate, Environmental Science and Pollution Research, 23, 6300–6311, https://doi.org/10.1007/s11356-015-5819-2, 2016.

Matsunaga, A., Docherty, K. S., Lim, Y. B., and Ziemann, P. J.: Composition and yields of secondary organic aerosol formed from OH radical-initiated reactions of linear alkenes in the presence of NOx: Modeling and measurements, Atmos Environ, 43, 1349–1357, https://doi.org/10.1016/j.atmosenv.2008.12.004, 2009.

McDonald, B. C., De Gouw, J. A., Gilman, J. B., Jathar, S. H., Akherati, A., Cappa, C. D., Jimenez, J. L., Lee-Taylor, J., Hayes, P. L., McKeen, S. A., Cui, Y. Y., Kim, S. W., Gentner, D. R., Isaacman-VanWertz, G., Goldstein, A. H., Harley, R. A., Frost, G. J., Roberts, J. M., Ryerson, T. B., and Trainer, M.: Volatile chemical products emerging as largest petrochemical source of urban organic emissions, Science (1979), 359, 760–764, https://doi.org/10.1126/science.aaq0524, 2018.

Nabi, D., Gros, J., Dimitriou-Christidis, P., and Arey, J. S.: Mapping environmental partitioning properties of nonpolar complex mixtures by use of GC × GC, Environ Sci Technol, 48, 6814–6826, https://doi.org/10.1021/es501674p, 2014.

Nimlos, M. R., Qian, X., Davis, M., Himmel, M. E., and Johnson, D. K.: Energetics of xylose decomposition as determined using quantum mechanics modeling, Journal of Physical Chemistry A, 110, 11824–11838, https://doi.org/10.1021/jp0626770, 2006.

Salvi, S. and Apte, K.: Household air pollution and its effects on health, F1000Res, 5, https://doi.org/10.12688/f1000research.7552.1, 2016.

Shah, R. U., Coggon, M. M., Gkatzelis, G. I., McDonald, B. C., Tasoglou, A., Huber, H., Gilman, J., Warneke, C., Robinson, A. L., and Presto, A. A.: Urban Oxidation Flow Reactor Measurements Reveal Significant Secondary Organic Aerosol Contributions from Volatile Emissions of Emerging Importance, Environ Sci Technol, 54, 714–725, https://doi.org/10.1021/acs.est.9b06531, 2020.

Shang, X., Pan, H., Li, M., Miao, X., and Ding, H.: Lonicera japonica Thunb.: Ethnopharmacology, phytochemistry and pharmacology of an important traditional Chinese medicine, https://doi.org/10.1016/j.jep.2011.08.016, 2011.

Silva, G. V., Martins, A. O., and Martins, S. D. S.: Indoor air quality: Assessment of dangerous substances in incense products, Int J Environ Res Public Health, 18, https://doi.org/10.3390/ijerph18158086, 2021.

Song, K., Guo, S., Gong, Y., Lv, D., Zhang, Y., Wan, Z., Li, T., Zhu, W., Wang, H., Yu, Y., Tan, R., Shen, R., Lu, S., Li, S., Chen, Y., and Hu, M.: Impact of cooking style and oil on semi-volatile and intermediate volatility organic compound emissions from Chinese domestic cooking, Atmos Chem Phys, 22, 9827–9841, https://doi.org/10.5194/ACP-22-9827-2022, 2022a.

Song, K., Gong, Y., Guo, S., Lv, D., Wang, H., Wan, Z., Yu, Y., Tang, R., Li, T., Tan, R., Zhu, W., Shen, R., and Lu, S.: Investigation of partition coefficients and fingerprints of atmospheric gas- and particle-phase intermediate volatility and semi-volatile organic compounds using pixel-based approaches, J Chromatogr A, 1665, 462808, https://doi.org/10.1016/j.chroma.2022.462808, 2022b.

Song, K., Guo, S., Gong, Y., Lv, D., Wan, Z., Zhang, Y., Fu, Z., Hu, K., and Lu, S.: Non-target scanning of organics from cooking emissions using comprehensive two-dimensional gas chromatography-mass spectrometer (GC×GC-MS), Applied Geochemistry, 151, https://doi.org/10.1016/j.apgeochem.2023.105601, 2023.

Staub, P. O., Schiestl, F. P., Leonti, M., and Weckerle, C. S.: Chemical analysis of incense smokes used in Shaxi, Southwest China: A novel methodological approach in ethnobotany, J Ethnopharmacol, 138, 212–218, https://doi.org/10.1016/j.jep.2011.08.078, 2011.

Stewart, G. J., Nelson, B. S., Acton, W. J. F., Vaughan, A. R., Hopkins, J. R., Yunus, S. S. M., Hewitt, C. N., Nemitz, E., Mandal, T. K., Gadi, R., Sahu, Lokesh. K., Rickard, A. R., Lee, J. D., and Hamilton, J. F.: Comprehensive organic emission profiles, secondary organic aerosol production potential, and OH

reactivity of domestic fuel combustion in Delhi, India, Environmental Science: Atmospheres, 1, 104–117, https://doi.org/10.1039/d0ea00009d, 2021.

Suzuki, S., Kiuchi, S., Kinoshita, K., Takeda, Y., Sakaida, S., Konno, M., Tanaka, K., and Oguma, M.: Formation of polycyclic aromatic hydrocarbons, benzofuran, and dibenzofuran in fuel-rich oxidation of toluene using a flow reactor, Physical Chemistry Chemical Physics, 23, 6509–6525, https://doi.org/10.1039/d0cp06615j, 2021.

Tang, R., Lu, Q., Guo, S., Wang, H., Song, K., Yu, Y., Tan, R., Liu, K., Shen, R., Chen, S., Zeng, L., Jorga, S. D., Zhang, Z., Zhang, W., Shuai, S., and Robinson, A. L.: Measurement report: Distinct emissions and volatility distribution of intermediate-volatility organic compounds from on-road Chinese gasoline vehicles: Implication of high secondary organic aerosol formation potential, Atmos Chem Phys, 21, 2569–2583, https://doi.org/10.5194/acp-21-2569-2021, 2021.

Tkacik, D. S., Presto, A. A., Donahue, N. M., and Robinson, A. L.: Secondary organic aerosol formation from intermediate-volatility organic compounds: Cyclic, linear, and branched alkanes, Environ Sci Technol, 46, 8773–8781, https://doi.org/10.1021/es301112c, 2012.

Tran, T. C. and Marriott, P. J.: Characterization of incense smoke by solid phase microextraction-Comprehensive two-dimensional gas chromatography (GC×GC), Atmos Environ, 41, 5756–5768, https://doi.org/10.1016/j.atmosenv.2007.02.030, 2007.

Uhde, E. and Salthammer, T.: Impact of reaction products from building materials and furnishings on indoor air quality-A review of recent advances in indoor chemistry, Atmos Environ, 41, 3111–3128, https://doi.org/10.1016/j.atmosenv.2006.05.082, 2007.

Wang, J., Jin, L., Gao, J., Shi, J., Zhao, Y., Liu, S., Jin, T., Bai, Z., and Wu, C. Y.: Investigation of speciated VOC in gasoline vehicular exhaust under ECE and EUDC test cycles, Science of the Total Environment, 445–446, 110–116, https://doi.org/10.1016/j.scitotenv.2012.12.044, 2013.

Wang, Y. and Qian, H.: Phthalates and their impacts on human health, https://doi.org/10.3390/healthcare9050603, 2021.

Wong, A., Lou, W., Ho, K. fai K., Yiu, B. K. fung, Lin, S., Chu, W. C. wing, Abrigo, J., Lee, D., Lam, B. Y. ka, Au, L. W. chi, Soo, Y. O. yan, Lau, A. Y. lun, Kwok, T. C. yui, Leung, T. W. hong, Lam, L. C. wa, Ho, K. fai K., and Mok, V. C. tong: Indoor incense burning impacts cognitive functions and brain

functional connectivity in community older adults, Sci Rep, 10, 1–11, https://doi.org/10.1038/s41598-020-63568-6, 2020.

Wu, W., Zhao, B., Wang, S., and Hao, J.: Ozone and secondary organic aerosol formation potential from anthropogenic volatile organic compounds emissions in China, J Environ Sci (China), 53, 224–237, https://doi.org/10.1016/j.jes.2016.03.025, 2017.

Yadav, V. K., Malik, P., Tirth, V., Khan, S. H., Yadav, K. K., Islam, S., Choudhary, N., Inwati, G. K., Arabi, A., Kim, D. H., and Jeon, B. H.: Health and Environmental Risks of Incense Smoke: Mechanistic Insights and Cumulative Evidence, J Inflamm Res, 15, 2665–2693, https://doi.org/10.2147/JIR.S347489, 2022.

Yang, T. T., Lin, T. S., and Chang, M.: Characteristics of emissions of volatile organic compounds from smoldering incense, Bull Environ Contam Toxicol, 78, 308–313, https://doi.org/10.1007/s00128-007-9184-9, 2007.

Yang, T. T., Ho, S. C., Chuang, L. te, Chuang, H. C., Li, Y. T., and Wu, J. J.: Characterization of particulate-phase polycyclic aromatic hydrocarbons emitted from incense burning and their bioreactivity in RAW264.7 macrophage, Environmental Pollution, 220, 1190–1198, https://doi.org/10.1016/j.envpol.2016.11.016, 2017.

Yu, Y., Guo, S., Wang, H., Shen, R., Zhu, W., Tan, R., Song, K., Zhang, Z., Li, S., Chen, Y., and Hu, M.: Importance of Semivolatile/Intermediate-Volatility Organic Compounds to Secondary Organic Aerosol Formation from Chinese Domestic Cooking Emissions, Environ Sci Technol Lett, https://doi.org/10.1021/acs.estlett.2c00207, 2022.

Yue, T., Yue, X., Chai, F., Hu, J., Lai, Y., He, L., and Zhu, R.: Characteristics of volatile organic compounds (VOCs) from the evaporative emissions of modern passenger cars, Atmos Environ, 151, 62–69, https://doi.org/10.1016/j.atmosenv.2016.12.008, 2017.

Zhao, Y., Hu, M., Slanina, S., and Zhang, Y.: Chemical compositions of fine particulate organic matter emitted from Chinese cooking, Environ Sci Technol, 41, 99–105, https://doi.org/10.1021/es0614518, 2007.

Zhao, Y., Hennigan, C. J., May, A. A., Tkacik, D. S., de Gouw, J. A., Gilman, J. B., Kuster, W. C., Borbon, A., and Robinson, A. L.: Intermediate-volatility organic compounds: A large source of

565 secondary organic aerosol, Environ Sci Technol, 48, 13743–13750, https://doi.org/10.1021/es5035188,
566 2014.
567 Zhao, Y., Nguyen, N. T., Presto, A. A., Hennigan, C. J., May, A. A., and Robinson, A. L.: Intermediate
568 Volatility Organic Compound Emissions from On-Road Diesel Vehicles: Chemical Composition,
569 Emission Factors, and Estimated Secondary Organic Aerosol Production, Environ Sci Technol, 49,
570 11516–11526, https://doi.org/10.1021/acs.est.5b02841, 2015.
571 Zhao, Y., Saleh, R., Saliba, G., Presto, A. A., Gordon, T. D., Drozd, G. T., Goldstein, A. H., Donahue,
572 N. M., and Robinson, A. L.: Reducing secondary organic aerosol formation from gasoline vehicle
573 exhaust, Proc Natl Acad Sci U S A, 114, 6984–6989, https://doi.org/10.1073/pnas.1620911114, 2017.
574 Zhu, X., Han, Y., Feng, Y., Cheng, P., Peng, Y., Wang, J., Cai, J., and Chen, Y.: Formation and emission
575 characteristics of intermediate volatile organic compounds (IVOCs) from the combustion of biomass
576 and their cellulose, hemicellulose, and lignin, Atmos Environ, 286, 119217,
577 https://doi.org/10.1016/j.atmosenv.2022.119217, 2022.
578 Zushi, Y., Yamatori, Y., Nagata, J., and Nabi, D.: Comprehensive two-dimensional
579 gas-chromatography-based property estimation to assess the fate and behavior of complex mixtures: A
580 case study of vehicle engine oil, Science of the Total Environment, 669, 739–745,
581 https://doi.org/10.1016/j.scitotenv.2019.03.157, 2019.
582

Figures

Figure 1. Volatility distributions of EF, OFP, and SOA with chemical class in each volatility bin. The *x*-axis is the unsaturated vapor concentration in logarithmic form (log C*, μg m^{-3}). The *y*-axis is the normalized mass emission factor (100%).

Figure 2. Positive (a) and negative loadings (b) of incense burning samples describing similarities and differences between chromatograms. The color bar is the loading.

Figure 3. Chemicals with high bioaccumulation potential (BAP) assesses by pixel-based approaches.

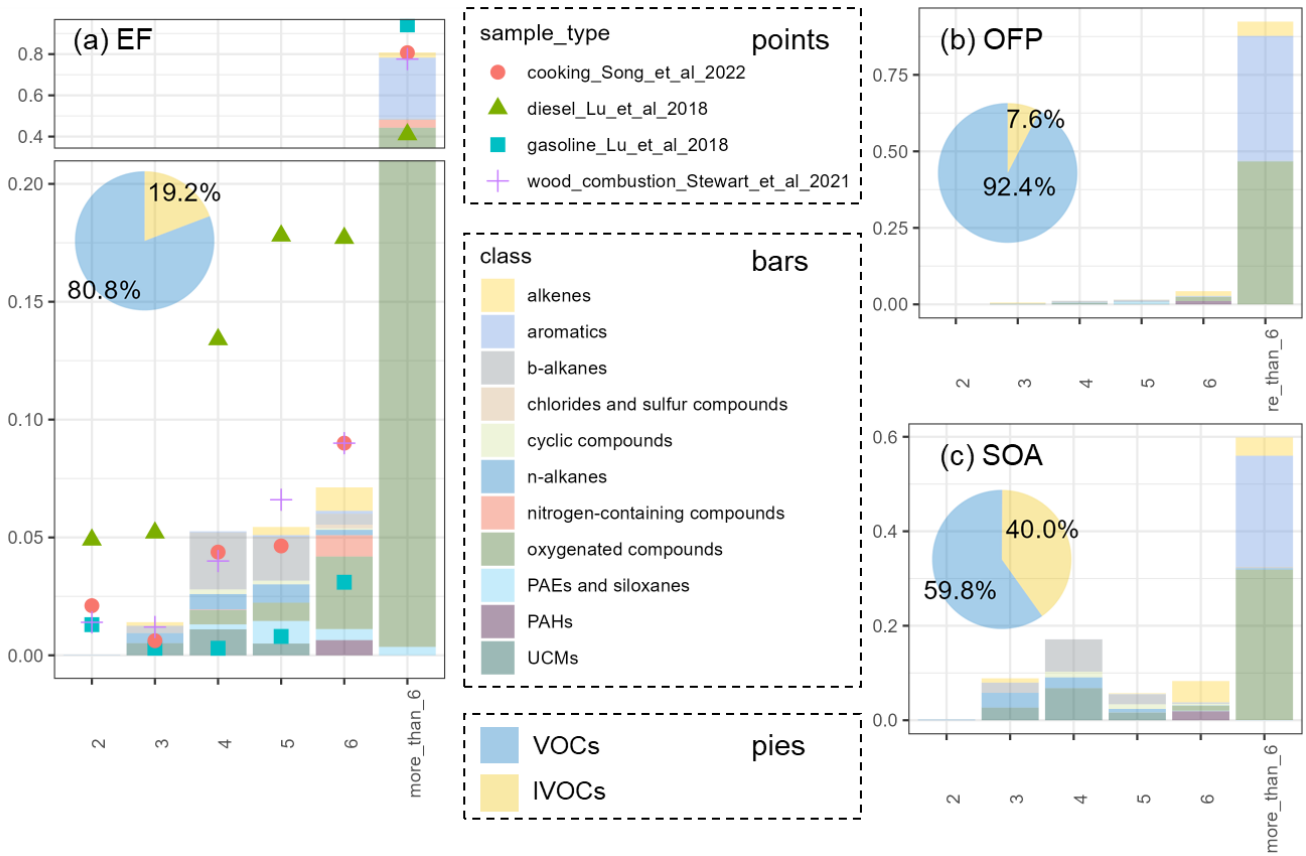

Figure 1. Volatility distributions of EF, OFP, and SOA with chemical class in each volatility bin. The *x*-axis is the unsaturated vapor concentration in logarithmic form (log C*, μg m^{-3}). The *y*-axis is the normalized mass emission factor (100%).

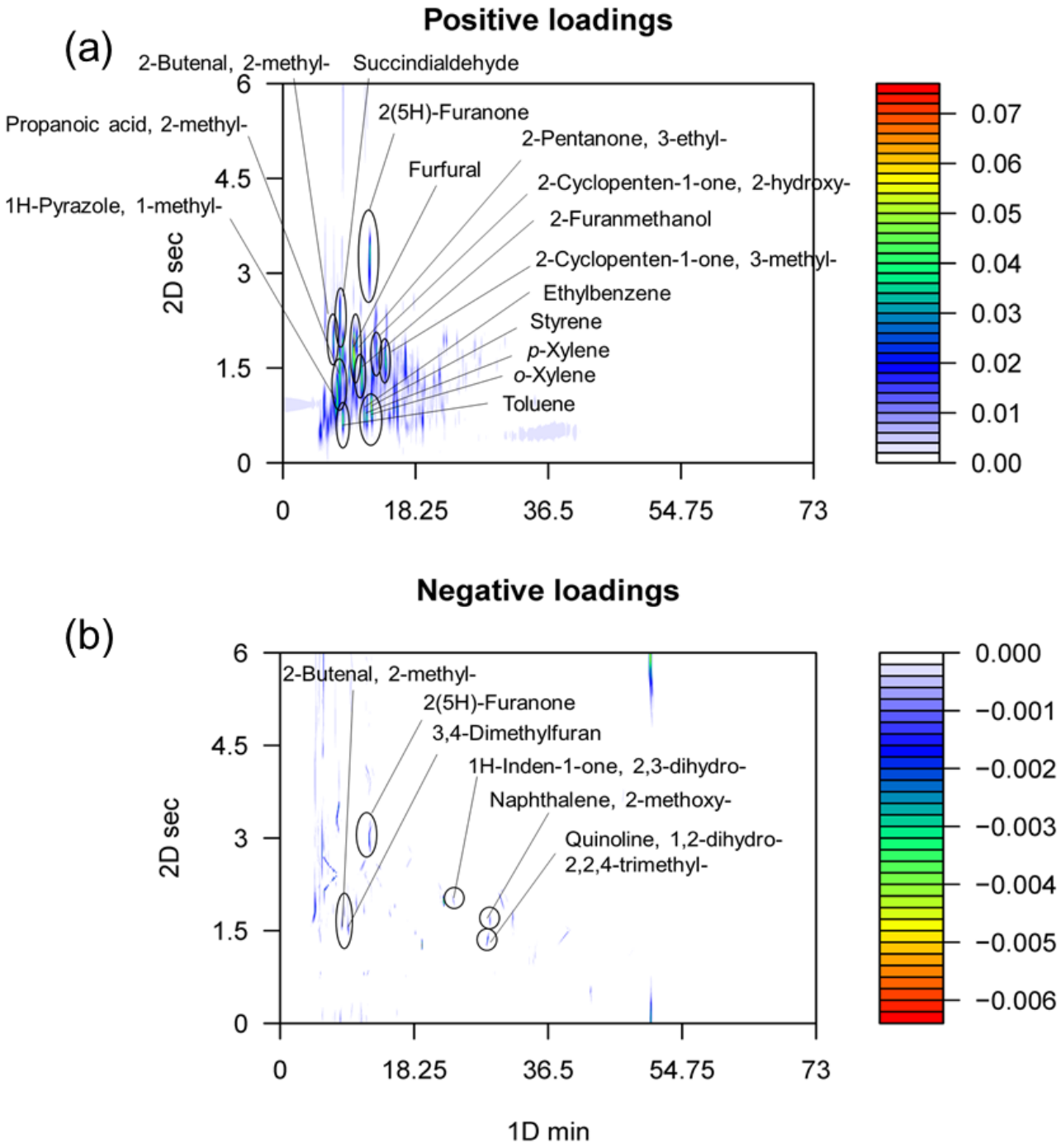

598

599 **Figure 2.** Positive (a) and negative loadings (b) of incense burning samples describing similarities

600 and differences between chromatograms. The color bar is the loading.

601

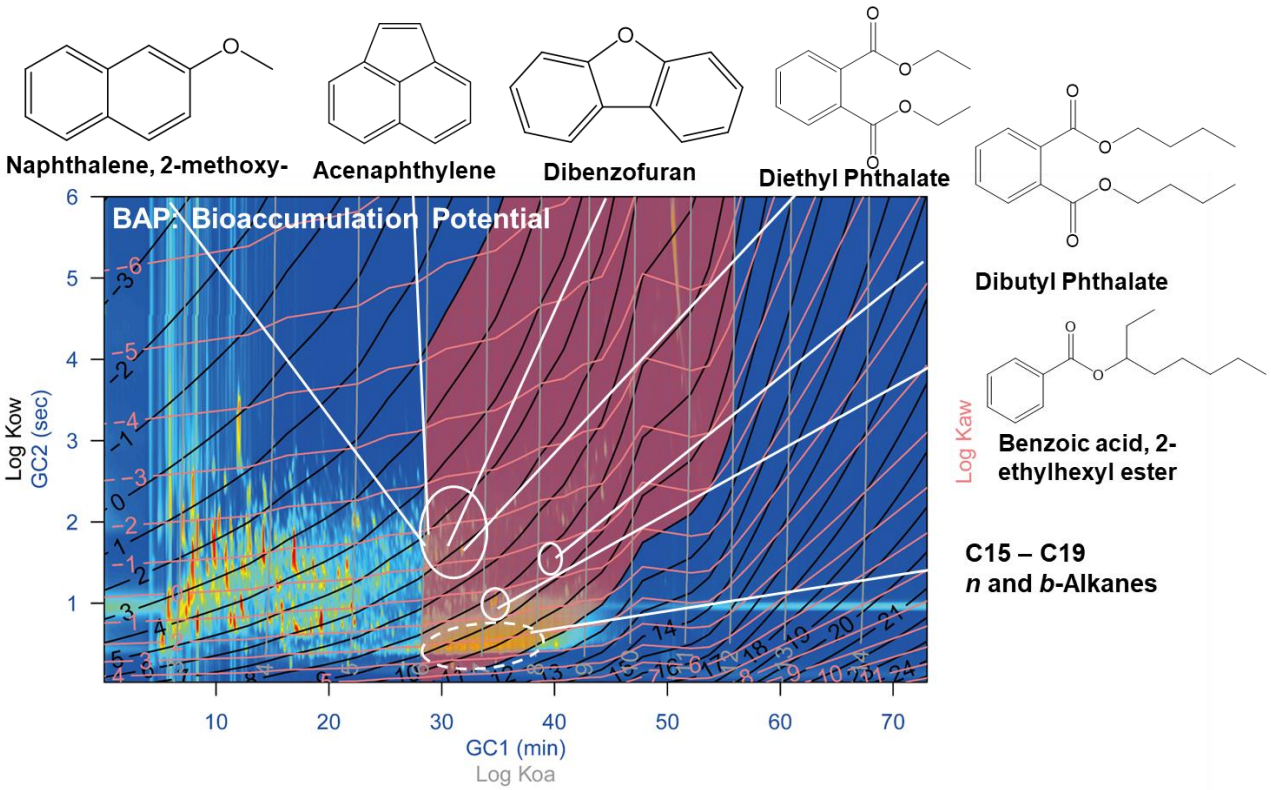

602

603 **Figure 3.** Chemicals with high bioaccumulation potential (BAP) assesses by pixel-based approaches.

604